Physica B 449 (2014) 121–128

Contents lists available at ScienceDirect

Physica B

journal homepage: www.elsevier.com/locate/physb

Non-perturbative study of impurity effects on the Kubo conductivity in macroscopic periodic and quasiperiodic lattices

Vicenta Sánchez [a], Carlos Ramírez [a], Fernando Sánchez [a], Chumin Wang [b,*]

[a] Departamento de Física, Facultad de Ciencias, Universidad Nacional Autónoma de México, Apartado Postal 70-542, 04510 México D.F., México
[b] Instituto de Investigaciones en Materiales, Universidad Nacional Autónoma de México, Apartado Postal 70-360, 04510 México D.F., Mexico

ARTICLE INFO

Article history:
Received 22 March 2014
Received in revised form
8 May 2014
Accepted 16 May 2014
Available online 22 May 2014

Keywords:
Electronic transport
Kubo–Greenwood formula
Renormalization method
Impurities in solids
Quasiperiodicity

ABSTRACT

In this paper, we analyze the effects of site and bond impurities on the electrical conductance of periodic and quasiperiodic systems with macroscopic length by means of a real-space renormalization plus a convolution method developed for the Kubo–Greenwood formula. All analyzed systems are connected to semi-infinite periodic leads. Analytical and numerical conductivity spectra are obtained for one and two site impurities in a periodic chain, where the separation between impurities determines the number of maximums in the spectra. We also found transparent states at the zero chemical potential in Fibonacci chains of every three generations with bond impurities, whose existence was confirmed by an analytical analysis within the Landauer formalism. For many impurities, the spectral average of the conductivity versus the system length reveals a power-law behavior, when the distance between impurities follows the Fibonacci sequence. Finally, we present an analysis of the conductance spectra of segmented periodic and Fibonacci chains and nanowires.

1. Introduction

One of the most basic topics in condensed matter physics beyond crystals is the presence of impurities in solids. They produce a wide variety of effects, particularly relevant in the conductivity, optical properties and specific heat. For example in nano-electronics, the effects of impurities are essential for the development of molecular devices such as novel computer architectures [1,2], chemical sensors [3] and biomedical sensors [4]. In fact, the inclusions of impurities in such systems could significantly alter the electronic transport, opening the possibility of design materials according to the requirements.

Nowadays, it is possible to create truly low-dimensional systems via a variety of methods, for example, by individually placing atoms one by one in a substrate [5,6]. Free-standing finite one-dimensional (1D) monoatomic chains of Ir [7], Pt [8], and Au [9–11] break junctions have been obtained. These systems would test theoretical results of low-dimensional systems. In particular, experimental data of the electronic transport through single atoms [12,13], molecules [14], and nanowires [15] have been reported.

Even though defects are virtually present in all solids, they are not easy to treat theoretically, since the presence of defects in a crystal breaks down the Bloch theorem and the reciprocal space. In the past, perturbative methods were frequently used for their analysis. For a more rigorous study of defects, it should be carried out in a full real space. However, the time necessary to solve quantum mechanical equations through conventional diagonalization methods grows cubically with the system size, making it computationally expensive to perform full real-space calculations. Consequently, only small clusters can be treated in an exact way by direct diagonalization or inversion methods. Nevertheless, the real-space renormalization procedure could be an efficient alternative, since the calculation time grows logarithmically with the number of atoms, making it possible to reach truly macroscopic systems.

In this article, we use a previously developed real-space renormalization method for the Kubo–Greenwood formula to analyze effects of site and bond impurities on the electrical conductivity in periodic and quasiperiodic systems, as well as in segmented nanowires.

2. The model

A typical one-dimensional quasiperiodic system is the Fibonacci chain, which can be modeled in different forms, for example, by using two sorts of bonds (bond problem), two kinds of atoms (site problem) or a combination of both (mixing problem) [16]. In this article, let us consider a bond problem consisting of null self-energies ($\varepsilon = 0$) and two hopping integrals, t_A and t_B, and they could follow the Fibonacci sequence (F_n) defined as $F_1 = A$, $F_2 = AB$ and $F_n = F_{n-1} \oplus F_{n-2}$. For example, $F_5 = ABAABABA$. For the case

* Corresponding author.
E-mail address: chumin@unam.mx (C. Wang).

http://dx.doi.org/10.1016/j.physb.2014.05.022
0921-4526/

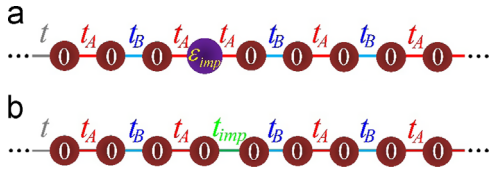

Fig. 1. Schematic representation of Fibonacci chains with a single (a) site and (b) bond impurity in the fourth position, corresponding to the border of Fibonacci chains of generation 3 and generation 2, as an example.

of periodic chains, we have $t_A = t_B$. We additionally include site (ε_{imp}) and bond (t_{imp}) impurities, as shown in Fig. 1 for the case of a single (a) site and (b) bond impurity located at the border of generation 3 and generation 2 of the Fibonacci chain connected to periodic leads with hopping integrals t. In order to isolate the quasicrystalline effects on physical properties, a single band tight-binding Hamiltonian is taken

$$H = \sum_j [\varepsilon_j |j\rangle\langle j| + t_{jj+1}|j\rangle\langle j+1| + t_{jj-1}|j\rangle\langle j-1|] \tag{1}$$

where $t_{jj\pm1}$ denotes the hopping integral between nearest-neighbor atoms and $|j\rangle$ are Wannier states.

It is well known that the electrical conductivity can be calculated within the linear response theory by using the Kubo–Greenwood formula given by [17]

$$\sigma(\mu,\omega,T) = \frac{2e^2\hbar}{\Omega\pi m^2}\int_{-\infty}^{\infty} dE \frac{f(E)-f(E+\hbar\omega)}{\hbar\omega} Tr[p\,\mathrm{Im}G^+(E+\hbar\omega)p\,\mathrm{Im}G^+(E)] \tag{2}$$

where Ω is the volume of the system, $G^+(E) = G(E+i\eta)$ is the retarded one-particle Green's function and $f(E) = \{1+\exp[(E-\mu)/(k_BT)]\}^{-1}$ is the Fermi–Dirac distribution with the Fermi energy $\mu$and temperature T, and p is the projection of the momentum operator along the applied electrical field, which for the Hamiltonian is given by Eq. (1) and $x = \sum_j x_j|j\rangle\langle j|$ can be expressed in terms of Wannier states as

$$p = \frac{im}{\hbar}[H,x] = \frac{ima}{\hbar}\sum_j \{t_{jj+1}|j\rangle\langle j+1| - t_{j-1j}|j\rangle\langle j-1|\}, \tag{3}$$

where a constant interatomic distance (a) is considered because the variation of interatomic distances can be absorbed by the parameters t_{jj+1}. As a limiting case of a periodic chain, when $T = 0$ and $\omega \to 0$, the conductivity is [18]

$$\sigma_P = \sigma(\mu,0,0) = \frac{e^2a}{\pi\hbar}(N-1), \tag{4}$$

where $\Omega = (N-1)a$ is the length of the system. In all the numerical calculations of this article, the impurities are included at the border of generations $n-1$ and $n-2$ when the Fibonacci chain of generation n is built, through the renormalization method for the Kubo–Greenwood formula developed in Ref. [19].

3. Conductivity in 1D systems

In Fig. 2, the electrical conductivity (σ) versus the chemical potential (μ) of a periodic chain with (a) site impurities of energy $\varepsilon_{imp} = 0.5|t|$ and (b) bond impurities with $t_{imp} = 0.5\,t$ is shown for the cases of one (red lines) and two (dark yellow lines) impurities. The number of atoms in these chains is $N = 433, 494, 438$, whose ends are connected to semi-infinite periodic leads with hopping integrals t. The imaginary part of the energy used in these calculations was $\eta = 10^{-13}|t|$. In general, the spectrum of a single impurity does not depend on the position of the impurity. For the case of two impurities, the spectrum depends only on the distance between them, which is chosen to be $512a$ in Fig. 2. Observe that the presence of a single impurity decreases the conductivity, but

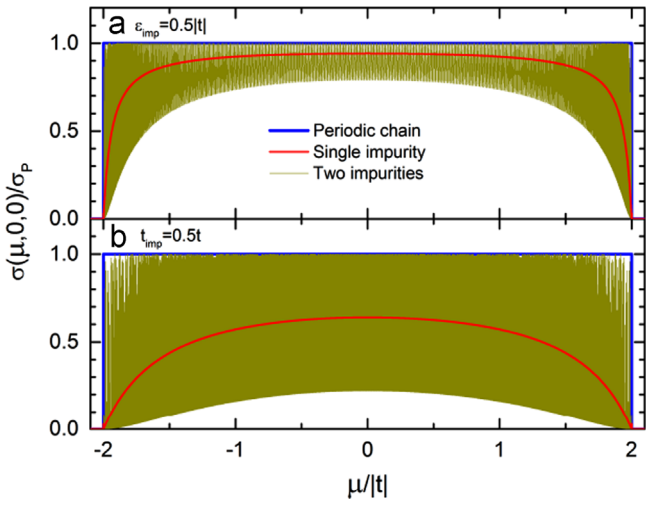

Fig. 2. Conductivity (σ) versus chemical potential (μ) spectra of a periodic chain with one (red lines) and two (dark yellow lines) impurities for the cases of (a) site and (b) bond impurities in comparison to that of a periodic chain without impurities (blue lines). (For interpretation of the references to color in this figure legend, the reader is referred to the web version of this article.)

such effect is more remarkable when the impurity is of bond nature. In both cases, the inclusion of two impurities produces a highly oscillating spectrum, whose amplitude is larger for bond impurities than for site ones. It is worth to mention that there is a localized state outside the band when we have site impurities, whose conductivity is very small in comparison with the conductivity spectrum and it can be visualized only in a logarithm scale due to the size of the system. The width of this conductivity peak depends on η, but the magnitude does not.

In order to obtain an analytic solution for the conductivity of a single impurity, we use the Landauer formula [20] in which for a single channel the electrical conductance $\boldsymbol{g}(\mu) = \boldsymbol{g}_0 T(\mu)$ being $\boldsymbol{g}_0 = 2e^2/h$. In consequence, the conductivity (σ) for one-dimensional chains is $\sigma(\mu) = \sigma_P\, T(\mu)$, whose transmittance ($T$) can be calculated by [18]

$$T(\mu) = \frac{4-(\mu/t)^2}{[\tau_{21}-\tau_{12}+(\tau_{22}-\tau_{11})\mu/2t]^2+(\tau_{22}+\tau_{11})^2(1-\mu^2/4t^2)} \tag{5}$$

where $\tau_{i,j}$ are elements of the transfer matrix

$$\boldsymbol{\tau}(\mu) = \begin{pmatrix} \tau_{11} & \tau_{12} \\ \tau_{21} & \tau_{22} \end{pmatrix} = \mathbf{T}_N\mathbf{T}_{N-1}\cdots\mathbf{T}_1 \text{ with}$$

$$\mathbf{T}_l = \begin{pmatrix} (\mu-\varepsilon_l)/t_{l,l+1} & -t_{l,l-1}/t_{l,l+1} \\ 1 & 0 \end{pmatrix}. \tag{6}$$

In particular, the transfer matrix ($\boldsymbol{\tau}_{imp}$) of a periodic chain with N atoms containing a single site impurity with energy ε_{imp} accomplishes

$$\boldsymbol{\tau}_{imp}(\mu,N) = \boldsymbol{\tau}(\mu,N) - \frac{\varepsilon_{imp}}{t}\boldsymbol{\tau}(\mu,N-1) - \frac{\varepsilon_{imp}}{t}\begin{pmatrix} \tau_{11}(\mu,N-3) & 0 \\ \tau_{11}(\mu,N-4) & 0 \end{pmatrix}, \tag{7}$$

where $\boldsymbol{\tau}(\mu,N)$ is the transfer matrix of a periodic chain of N atoms without impurities, whose first element satisfies

$$\tau_{11}^2(\mu,N) + \tau_{11}^2(\mu,N-1) - \mu\,\tau_{11}(\mu,N)\,\tau_{11}(\mu,N-1)/t = 1. \tag{8}$$

Therefore, the transmittance of a periodic chain with N atoms and a single site impurity with energy ε_{imp} is

$$T(\mu) = \frac{4-(\mu/t)^2}{4-(\mu/t)^2+(\varepsilon_{imp}/t)^2}. \tag{9}$$

Notice that the red curve of Fig. 2(a) inside the band can be alternatively obtained from Eq. (9).

In addition, Fig. 2 shows that the conductivity spectra of two impurities are composed of many resonant peaks, whose number is the number of atoms between these two impurities. This fact can be better seen in Fig. 3 for the cases of (a) 5, (b) 13 and (c) 60 atoms between site impurities with $\varepsilon_{imp}=0.5|t|$ and for the cases of (d) 6, (e) 16 and (f) 64 atoms between bond impurities with $t_{imp}=0.5t$. In all the cases, the system size and η are the same as in Fig. 2. For the case of site impurities, the spectrum is asymmetric with respect to the zero chemical potential and has always a peak of conductivity outside the band at $\mu>2|t|$. In contrast, for bond impurities, the spectrum remains symmetrical because the lattice is bipartite.

In order to verify analytically the conductivity of a periodic chain with two site impurities, whose transfer matrix can be written as $\boldsymbol{\tau}_{2imp}(\mu,N)=\boldsymbol{\tau}_{imp}(\mu,N)\boldsymbol{\tau}_{imp}(\mu,N)$, we obtain the transmittance given by

$$T(\mu,N)=\frac{4-\varepsilon^2}{4-\varepsilon^2+4\tilde{\varepsilon}^2+\tilde{\varepsilon}^2(\tilde{\varepsilon}^2-2\tilde{\varepsilon}\varepsilon+\varepsilon^2-4)\tau_{11}^2(N-1)+4\tilde{\varepsilon}^3\tau_{11}(N-1)\tau_{11}(N-2).} \tag{10}$$

where $\varepsilon=\mu/t$, $\tilde{\varepsilon}=\varepsilon_{imp}/t$ and $\tau_{11}(N)=\sum_{l=0}^{\lfloor N/2\rfloor}(-1)^l(N-l)!\varepsilon^{N-2l}/[l!(N-2l)!]$.

The conductivity of Fig. 3(a) and (b) obtained by means of real-space renormalization methods coincides with the analytical solution given by Eq. (10). Moreover, Fig. 3(a) is similar to that presented in Ref. [21, Fig. 2], while Fig. 3(d) is similar to that reported in Ref. [22, Fig. 6].

The position of conductivity resonant peaks for the case of two bond impurities depend on the value of t_{imp}. In particular, when $t_{imp}\to 0$, these peaks are located at the eigenvalues of a periodic chain with N_{i-i} atoms, being N_{i-i} the number of atoms between these two bond impurities. For finite values of t_{imp}, the position of the resonant peaks follows the relation:

$$E_k(t_{imp},N_{i-i})=E_k(0,N_{i-i})+a_k(N_{i-i})\,t_{imp}^2+b_k(N_{i-i})\,t_{imp}^3. \tag{11}$$

where k enumerates each peak, $E_k(0,N_{i-i})$ is the corresponding eigenvalue of the periodic chain with N_{i-i} atoms, $a_k(N_{i-i})=A_kN_{i-i}^{-\alpha_k}$ and $b_k(N_{i-i})=B_kN_{i-i}^{-\beta_k}$, being A_k, B_k, α_k and β_k constants.

Fig. 4 shows the dependence of electrical conductivity (in color scale) on ε_{imp} and t_{imp} for a single impurity in the same systems of Fig. 2. Notice that the conductivity spectrum of Fig. 4(a) is symmetrical with respect to $\varepsilon_{imp}=0$ for the site impurity case and asymmetric around $t_{imp}=t$ in the bond impurity one.

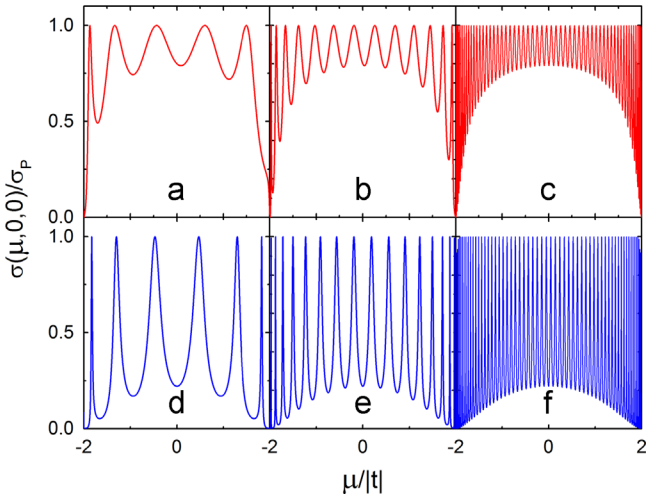

Fig. 3. Conductivity (σ) versus chemical potential (μ) spectra of a periodic chain with two site impurities separated by (a) 5 (b) 13 and (c) 60 atoms, and two bond impurities separated by (d) 6, (e) 16 and (f) 64 atoms, using the same parameters of Fig. 2.

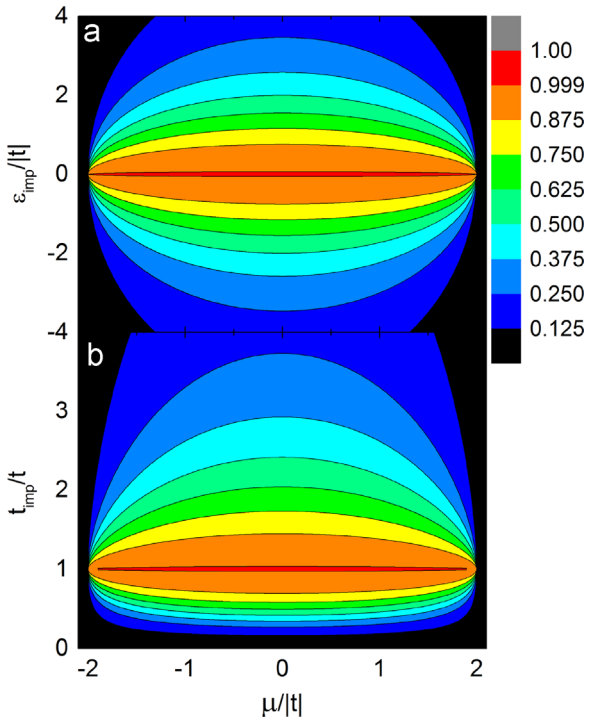

Fig. 4. Conductivity spectra (in color scale) of a periodic chain with a single (a) site or (b) bond impurity as a function of the chemical potential (μ) and ε_{imp} or t_{imp} for the same systems of Fig. 2. (For interpretation of the references to color in this figure legend, the reader is referred to the web version of this article.)

By comparing Fig. 4(a) and (b), we observe that the conductivity is more (less) suppressed when the impurity is caused by a bond impurity with t_{imp} smaller (larger) than one. Particularly, the conductivity is null for t_{imp} close to zero.

Fig. 5 shows the dependence of electrical conductivity (in color scale) on (a) ε_{imp} and (b) t_{imp} for the same systems of Fig. 3(b) and (e), respectively. Notice that Fig. 5(a) is asymmetric with respect to the zero chemical potential, contrary to the symmetry observed in Fig. 5(b) which is in turn asymmetric with respect to $t_{imp}=t$. In both cases, the conductivity is almost null if the values of ε_{imp} or t_{imp} are very different from 0 or t correspondingly. It is worth to mention that when $|t_{imp}/t|>1$ we found two localized states outside the band, symmetrically placed with respect to the zero chemical potential, whose width depends on η but its magnitude does not.

Fig. 6 shows electrical conductivity (σ) of Fibonacci chains with hopping integrals $t_A=0.9\,t$, $t_B=t$ and (a) one site impurity (red lines), (b) two site impurities separated by 512 atoms (red lines), (c) two site impurities separated 1024 atoms (red lines), (d) one bond impurity (blue lines), (e) two bond impurities separated 512 atoms (blue lines) and (f) two bond impurities separated 1024 atoms (blue lines), using the same N and η of Fig. 2 and $\varepsilon_{imp}=|t|$ or $t_{imp}=0.3\,t$. All these spectra are compared to that of the Fibonacci chain without impurities (gray lines). Observe that for site impurities the spectra are asymmetric with respect to the zero chemical potential, which is even noticeable for the case of a single site impurity as shown in Fig. 6(a), contrary to the periodic case given by Eq. (9). In general, the diminution of conductivity is less for site than for bond impurities.

It is well known that the bond-Fibonacci chains have a transparent state (transmission coefficient equal to one) at the zero chemical potential every six generations [19]. This fact does not remain for long when site or bond impurities are present. In particular, site impurities always destroy the transparent state at the zero chemical potential in bond-Fibonacci chains. On the other

hand, bond impurities only annihilate this transparent state when the number of such impurities is odd for any value of the hopping t_{imp}, while an even number of them makes the apparition of transparent states every three generations when $t_{imp} = t_B$ substitutes a t_A bond. This fact can be verified by observing that the transfer matrix elements (i,j) as a function of the generation (n) can be written as

$$\tau_{i,j}(n) = (-1)^{n+i}\left[\gamma^{f(n)}\frac{t_{imp}}{t_B}\right]^{(j-i)}\delta_{3,i+j}\,\delta_{x,2} + \left\{(-1)^{n+1}\left[\gamma^{f(n)}\frac{t_{imp}}{t_A}\right]^{(3-2i)}\delta_{x,0} - \left(\frac{t_{imp}}{t_B}\right)^{(3-2i)}\delta_{x,1}\right\}\delta_{0,i-j}, \tag{12}$$

where $x = n \pmod 3$, $f(n) = 1-(-1)^n$ and $\gamma = t_A/t_B$. The corresponding transmittance is

$$T(\mu=0,n) = \frac{4}{[(\gamma^{-f(n)}(t_{imp}/t_B))+((t_B/t_{imp})\gamma^{f(n)})]^2\delta_{x,2}+[(\gamma^{f(n)}(t_{imp}/t_A))+((t_A/t_{imp})\gamma^{-f(n)})]^2\delta_{x,0}+[(t_{imp}/t_B)+(t_B/t_{imp})]^2\delta_{x,1}}. \tag{13}$$

From Eq. (13) we conclude that $T(\mu=0,n)=1$ when $t_{imp} = t_B$ and $x=1$.

Recently, segmented nanowires were fabricated and they possess unique properties [23]. Hence, we further study segmented periodic and Fibonacci chains, which can be built by joining blocks of atoms and ordering them following a periodic or Fibonacci sequence, as shown in Fig. 7. The corresponding periodic and quasiperiodic nanowires with finite cross section will be analyzed in the next section.

Fig. 8 shows the conductivity (σ) versus chemical potential (μ) spectra for a segmented periodic chain of 144,946,903 atoms, blocks of four atoms ($N_A = N_B = 4$), $\eta = 10^{-13}|t|$, hopping integrals $t_B = t$ and (a) $t_A = 0.9\,t$, (b) $t_A = 0.8\,t$, (c) $t_A = 0.7t$ and (d) $t_A = 0.6\,t$. Notice that a larger difference between t_A and t_B produces wider energy gaps in the conductivity spectra and the number of band depends on the total number of bonds in the unitary cell. For example, in Fig. 8 there are six conductivity bands, because we have three bonds in each block.

The conductivity spectra of a segmented Fibonacci chain with 117,264,508 atoms are shown in Fig. 9(a–d) with the same parameters of Fig. 8(a–d), while Fig. 9(e–h) corresponds to conductivity spectra of bond-Fibonacci chains without block structure ($N_A = N_B = 2$). It is observed that when the difference between t_A and t_B increases, the band width diminishes. Moreover, there are more high-conductivity states in segmented Fibonacci chains than in the corresponding Fibonacci chain without block structure.

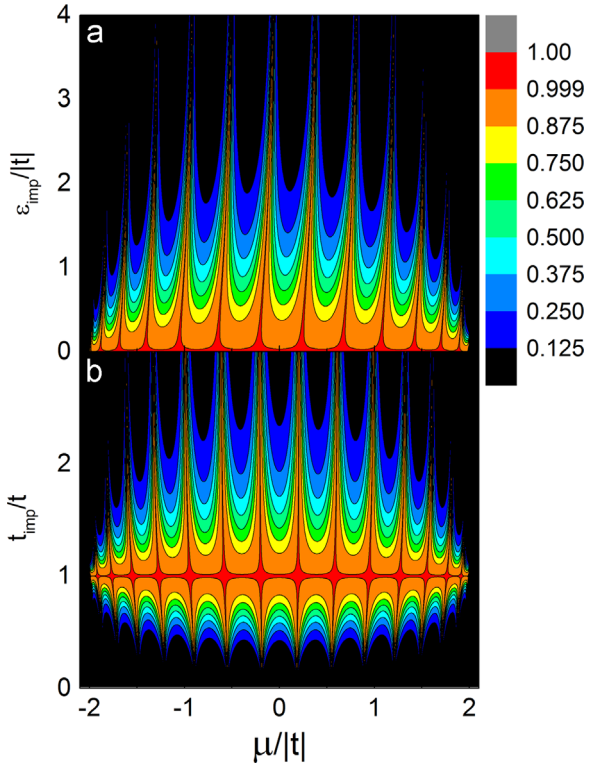

Fig. 5. Conductivity spectra (in color scale) of a periodic chain with two (a) sites or (b) bond impurities as a function of the chemical potential (μ) and ε_{imp} or t_{imp} for the system of Fig. 3(b) and (e), respectively. (For interpretation of the references to color in this figure legend,the reader is referred to the web version of this article.)

In order to analyze the global behavior of systems studied in this section, we present in Fig. 10 spectral averages of the conductivity $(<\sigma>)$ given by

$$<\sigma> = \frac{\int \sigma(\mu,0,0)DOS(\mu)d\mu}{\int DOS(\mu)d\mu}, \tag{14}$$

for segmented periodic chains with blocks of four (blue open triangles) and 90 (blue open squares) atoms, and periodic chains with 377 site (magenta solid circles) and bond (red open circles) impurities. The parameters of this figure are $t_A = t_{imp} = 0.7t$, $t_B = t$, $\varepsilon_{imp} = 0.7|t|$ and $\eta = 10^{-15}|t|$. The numerical integration was performed by using the Simpson algorithm with a fixed step of $\Delta\mu = 5\times10^{-7}|t|$. Site and bond impurities are introduced in such a way that the distance between impurities follows the Fibonacci sequence. For instance, in the case of 377 site impurities in a periodic chain of 1598 atoms, the distance between impurities is $d_A = 5\,a$ and $d_B = 3\,a$. Let us put the first impurity at the fourth

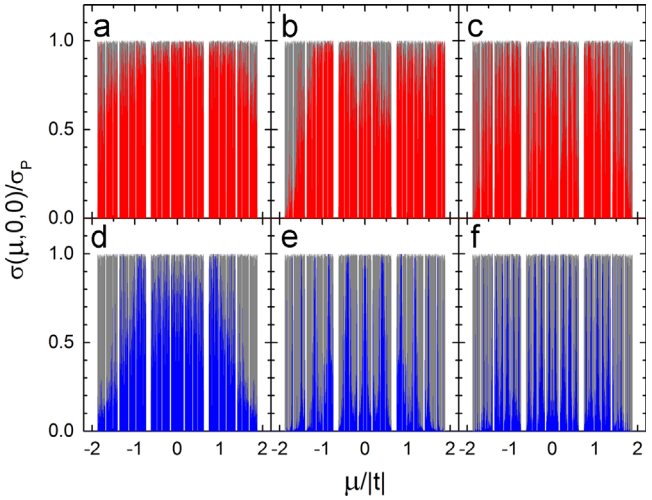

Fig. 6. Conductivity (σ) versus chemical potential (μ) spectra of Fibonacci chains with (a) one, (b) two separated by 512 atoms, (c) two separated by 1024 atoms site impurities (red lines), (d) one, (e) two separated by 512 atoms and (f) two separated by 1024 atoms bond impurities (blue lines), in comparison to that of the Fibonacci chain without impurities (gray lines). All the systems have $t_A = 0.9\,t$ and $t_B = t$. (For interpretation of the references to color in this figure legend, the reader is referred to the web version of this article.)

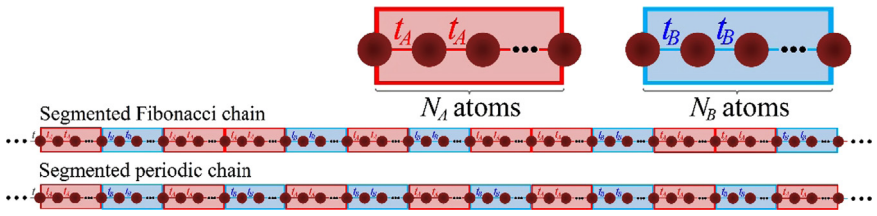

Fig. 7. Schematic representation of segmented Fibonacci and periodic chains. Each block contains $N_A - 1$ *A*-type bonds or $N_B - 1$ *B*-type bonds.

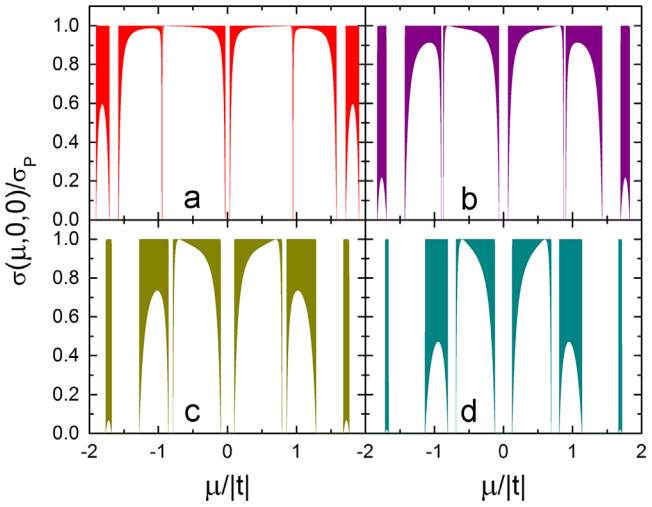

Fig. 8. Conductivity (σ) versus chemical potential (μ) spectra of a segmented periodic chain with blocks of $N_A = N_B = 4$ atoms, $t_B = t$ and (a) $t_A = 0.9\,t$, (b) $t_A = 0.8\,t$, (c) $t_A = 0.7t$and (d) $t_A = 0.6\,t$.

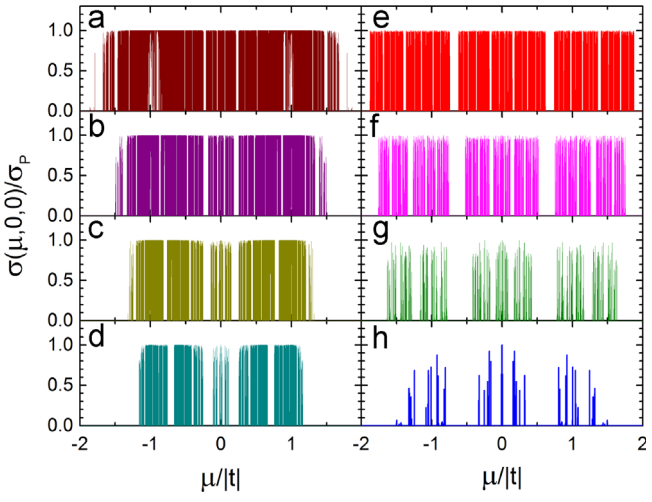

Fig. 9. Conductivity (σ) versus chemical potential (μ) spectra of a segmented Fibonacci chain with blocks of $N_A = N_B = 4$ bonds, $t_B = t$ and (a) $t_A = 0.9\,t$, (b) $t_A = 0.8\,t$, (c) $t_A = 0.7t$and (d) $t_A = 0.6\,t$ in comparison to the corresponding Fibonacci chains without block structure ($N_A = N_B = 2$) for $t_B = t$ and (e) $t_A = 0.9\,t$, (f) $t_A = 0.8\,t$, (g) $t_A = 0.7t$and (h) $t_A = 0.6\,t$.

atom, the second one at the ninth atom, the third one at the twelfth atom, and next impurities are located following the Fibonacci sequence; for example, the eighth impurity is located at a distance of $d_A + d_B + d_A + d_A + d_B + d_A + d_B = 29a$ from the first impurity.

Notice in Fig. 10 that $<\sigma>/\sigma_P$ is unity for any number of atoms in a periodic chain (gray balls). This constant behavior remains for segmented periodic chains, having only small fluctuations when the number of atoms is low, because we have extended wave functions. For chains with bond or site impurities located

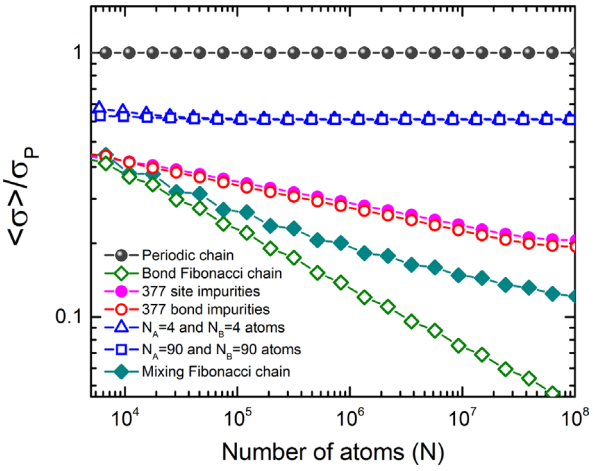

Fig. 10. Spectral average of the conductivity ($<\sigma>$) as a function of the number of atoms (N) in segmented periodic chains with blocks of four (blue open triangles) and 90 (blue open squares) atoms, periodic chains with 377 site (magenta solid circles) and bond (red open circles) impurities, in comparison to $<\sigma>$ of pure periodic (gray solid balls), bond (green open rhombs) and mixing (dark cyan solid rhombs) Fibonacci chains. (For interpretation of the references to color in this figure legend, the reader is referred to the web version of this article.)

after the Fibonacci sequence, $<\sigma>$ decays with the number of atoms following a power law ($<\sigma> \propto N^{-s}$) with a smaller exponent (s) in comparison to the pure Fibonacci chain (green rhombs), whose s is a function of $\gamma = t_A/t_B$. This power-law behavior is related to the critical nature of wavefunctions [24]. It would be worth mentioning that fluctuations observed in the results of the pure Fibonacci chains and at the end of impurity cases could be due to the finite value of $\Delta\mu$ in the Simpson integration.

In Fig. 10, we also present $<\sigma>$ for a mixed Fibonacci chain (dark cyan solid rhombs) whose sites follow the Fibonacci sequence. For example, for generation five the chain is ABAABABA, where A and B indicate the nature of atoms with self-energies ε_A and ε_B, respectively. In consequence, the bonds of this chain are ordered as $t_I t_I t_{AA} t_I t_I t_I t_I$, where t_I (t_{AA}) is the hoping integral between atoms A and B (A and A). In particular, $<\sigma>$ of a mixing Fibonacci chain was calculated by means of the renormalization method described in Ref. [25] using the parameters $\varepsilon_A = \varepsilon_B = 0$, $t_{AA} = 0.7t$, $t_I = t$ and the same η and $\Delta\mu$. It is worth to mention that the ratio between the numbers of t_I and of t_{AA} is 2τ when the chain length tends to infinite, being $\tau = (\sqrt{5}+1)/2$ the golden mean. Notice that $<\sigma>$ of the mixing problem as a function of the system length decays following an almost power law, since its ordering of bonds does not satisfy the quasiperiodic criteria [26].

4. Electrical conductance of nanowires

This study is further extended to quantify the effects of impurities in nanowires, whose conductance (g) can be calculated by $g(E) = \sigma(E)W/L$, where L is the length and W is the cross sectional area of the sample. In general, electrical conductance is

commonly expressed in units of $g_0 = 2e^2/h$. All the nanowires analyzed in this section have the same hopping integral t in the transversal planes. In Fig. 11, the electrical conductance of a periodic nanowire with $N = 433,494,438 \times 6 \times 6$ atoms is illustrated, using $\eta = 10^{-15}|t|$, for the cases of (a) one plane of site impurities, (b) two planes of site impurities, (c) one plane of bond impurities and (d) two planes of bond impurities, taking correspondingly $\varepsilon_{imp} = 0.2|t|$ (blue lines), $0.3|t|$ (green lines), $0.4|t|$ (dark yellow lines), $0.5|t|$ (magenta lines), $0.6|t|$ (orange lines) and $0.7|t|$, (violet lines); or $t_{imp} = 0.7t$ (violet lines), $0.6\,t$ (orange lines), $0.5\,t$ (magenta lines), $0.4\,t$ (dark yellow lines), $0.3\,t$ (green lines) and $0.2\,t$ (blue lines). A sketch of plane impurities can be found in Ref. [27, Fig. 1]. In addition, the conductance spectrum of the corresponding periodic nanowire without impurities is shown as gray lines. Observe that when a single plane of site or bond impurities is introduced, the quantized conductance spectra of pure periodic systems are smoothed and decreases when ε_{imp} grows or t_{imp} reduces. In fact, this effect is more remarkable when the impurity is of bond nature. For the case of two planes of impurities, oscillating spectra are found. Notice that the conductance spectrum of two site-impurity planes is lower than that of a single plane of site impurities. Such a fact is not found for planes of bond impurities.

Fig. 12 shows the electrical conductance (g) as a function of chemical potential (μ) varying the on-site impurity energy (ε_{imp}) from 0 to $4|t|$, for the same nanowires of Fig. 11 with (a) one site-impurity plane, two site-impurity planes separated by (b) 13 atoms and (c) 60 atoms. Notice that the conductance spectra are asymmetric with respect to the zero chemical potential for the cases of two site-impurity planes. Moreover, the quantization of the conductance is destroyed if the number of impurity planes, the distance between them or ε_{imp} increase. When the number of site-impurity planes is greater than one, the conductance spectra become composed by very thin peaks, observed as black lines in Fig. 12(b) and (c). For negative values of ε_{imp}, we always obtain antisymmetric spectra with respect to $\varepsilon_{imp} = 0$.

For the case of bond impurities, similar results of Fig. 12 are shown in Fig. 13 for nanowires with (a) one bond-impurity plane, two bond-impurity planes separated by (b) 16 and (c) 64 atoms, whose impurity hoping integrals (t_{imp}) vary between 0 and $3\,t$. In contrast to Fig. 12, the conductance spectra is symmetric around the zero chemical potential. Furthermore, the conductance is more rapidly diminished when $t_{imp}/t < 1$ in comparison to $t_{imp}/t > 1$.

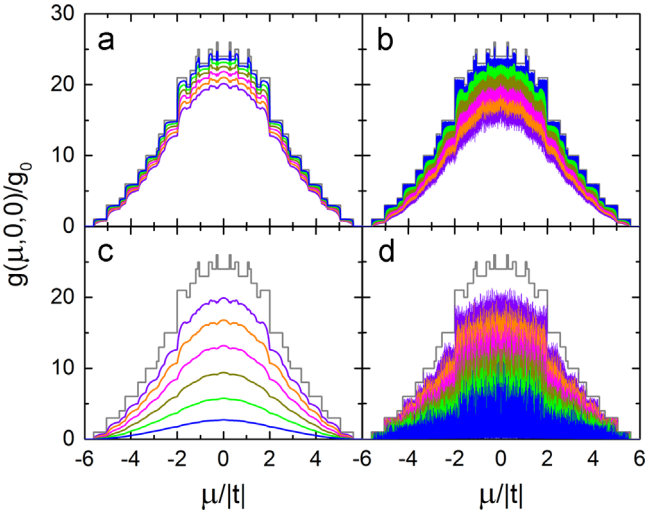

Fig. 11. Conductance (g) versus chemical potential (μ) spectra of periodic nanowires of $N = 433494438 \times 6 \times 6$ atoms containing (a) one site-impurity plane, (b) two site-impurity planes, (c) one bond-impurity plane and (d) two bond-impurity planes, taking $\varepsilon_{imp} = 0.2|t|$ (blue lines), $0.3|t|$ (green lines), $0.4|t|$ (dark yellow lines), $0.5|t|$ (magenta lines), $0.6|t|$ (orange lines) and $0.7|t|$, (violet lines); or $t_{imp} = 0.7t$ (violet lines), $0.6\,t$ (orange lines), $0.5\,t$ (magenta lines), $0.4\,t$ (dark yellow lines), $0.3\,t$ (green lines), $0.2\,t$ (blue lines), and $\eta = 10^{-15}|t|$. (For interpretation of the references to color in this figure legend, the reader is referred to the web version of this article.)

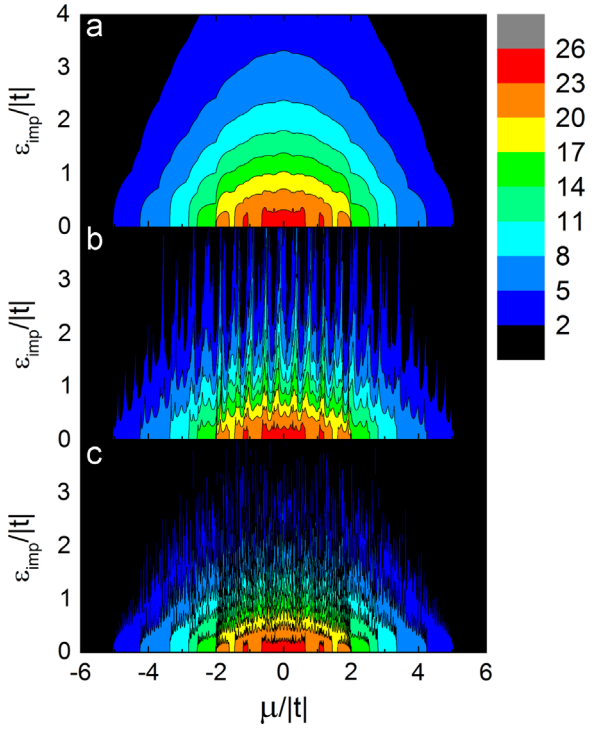

Fig. 12. Conductance (g) spectra as functions of the chemical potential (μ) and the on-site impurity energy (ε_{imp}) for periodic nanowires with (a) one site-impurity plane, two site-impurity planes separated by (b) 13 atoms and (c) 60 atoms.

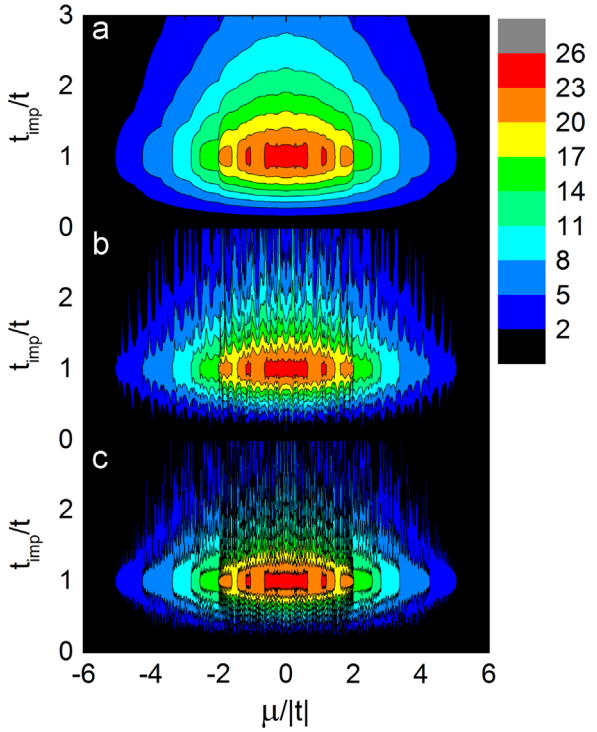

Fig. 13. Conductance (g) spectra as functions of the chemical potential (μ) and the impurity hopping integral (t_{imp}) for periodic nanowires with (a) one bond-impurity plane, two bond-impurity planes separated by (b) 13 atoms and (c) 60 atoms.

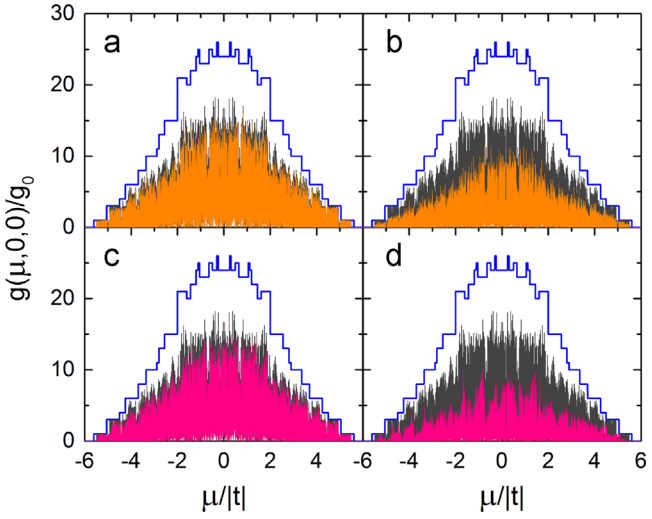

Fig. 14. Conductance (g) spectra as functions of chemical potential (μ) for Fibonacci nanowires containing one site-impurity plane with (a) $\varepsilon_{imp}=0.5|t|$ and (b) $\varepsilon_{imp}=1.5|t|$, as well as two site-impurity planes separated by 64 atoms with (c) $\varepsilon_{imp}=0.5|t|$ and (d) $\varepsilon_{imp}=1.5|t|$, in comparison to the conductance spectra of periodic (blue lines) and Fibonacci (gray lines) nanowires without impurities. (For interpretation of the references to color in this figure legend, the reader is referred to the web version of this article.)

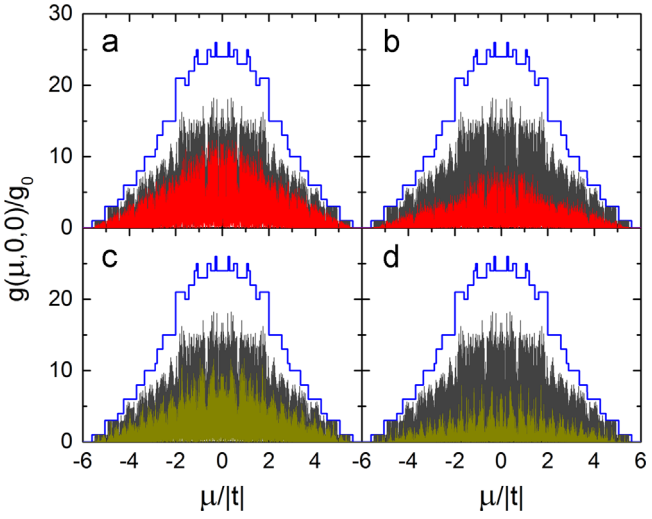

Fig. 15. Conductance (g) spectra as functions of the chemical potential (μ) for Fibonacci nanowires containing one bond-impurity plane with (a) $t_{imp}=0.5t$, (b) $t_{imp}=0.3t$, two bond-impurity planes separated by 64 atoms with (c) $t_{imp}=0.5t$ and (d) $t_{imp}=0.3t$, in comparison to the conductance spectra of periodic (blue lines) and Fibonacci (gray lines) nanowires without impurities. (For interpretation of the references to color in this figure legend, the reader is referred to the web version of this article.)

In similitude to the site-impurity cases of Fig. 12, the conductance quantization is also quickly destroyed when the number of impurity planes or the distance between them increase.

We further extend this study to quasiperiodic nanowires. In Fig. 14, the conductance spectra are shown for nanowires of $N=433,494,438\times 6\times 6$ atoms, whose hopping integrals $t_A=0.9\,t$ and $t_B=t$ along the longitudinal axis follow the Fibonacci sequence, $\eta=10^{-15}|t|$, and one site-impurity plane with (a) $\varepsilon_{imp}=0.5|t|$, (b) $\varepsilon_{imp}=1.5|t|$, and two site-impurity planes separated by 64 atoms with (c) $\varepsilon_{imp}=0.5|t|$ and (d) $\varepsilon_{imp}=1.5|t|$. These spectra are compared with those of a periodic (blue line) and of a Fibonacci nanowire without impurities (gray line). Notice that these conductance spectra of quasiperiodic nanowires are always asymmetric for any number of impurity planes. Moreover, the conductance diminish when ε_{imp} increases.

In parallel to Fig. 14 for site-impurity cases, Fig. 15 reveals the conductance spectra of Fibonacci nanowires containing one bond-impurity plane with (a) $t_{imp}=0.5\,t$, (b) $t_{imp}=0.3\,t$, two bond-impurity planes separated by 64 atoms with (c) $t_{imp}=0.5\,t$ and (d) $t_{imp}=0.3\,t$. The same parameters of Fig. 14 are used in the calculations for Fig. 15 and the obtained conductance spectra are also compared to those of periodic (blue line) and Fibonacci (gray line) nanowires without impurities. Observe that the conductance quickly decrease when t_{imp} diminishes for any number of impurities. It is worth to mention that while the separation between bond-impurity planes is larger, the decrease of the conductance is slower. The inclusion of bond-impurity planes with $t_{imp}/t<1$ has significantly stronger effects over the conductance spectra of Fibonacci nanowires than the addition of site impurities, as occurs in periodic nanowires.

For the case of segmented nanowires, Fig. 16 shows their conductance spectra versus the chemical potential of periodically segmented nanowires with blocks containing four atoms, total number of atoms $N=144,946,903\times 6\times 6$, $\eta=10^{-15}t$, $t_B=t$ and (a) $t_A=0.9\,t$, (b) $t_A=0.8\,t$, (c) $t_A=0.7t$ and (d) $t_A=0.6\,t$. It can be noticed that the quantized spectrum behavior is still preserved in the case (a) but not in the other cases, where such quantization is only present in both band extremes.

On the other hand, in Fig. 17 the electrical conductance spectra are illustrated for quasiperiodically segmented nanowires whose

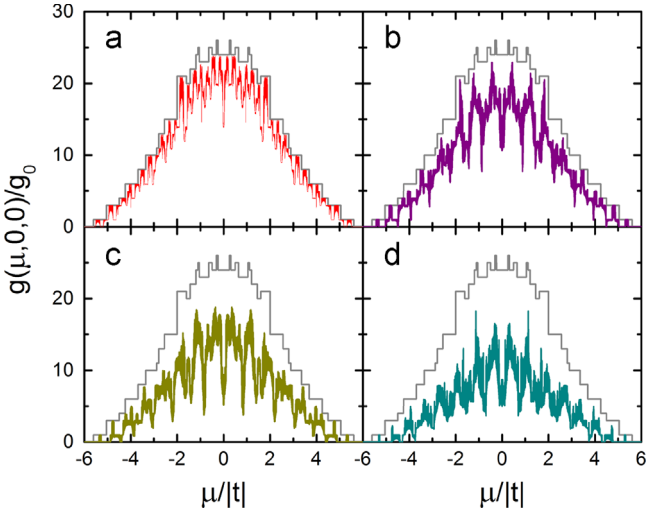

Fig. 16. Conductance (g) spectra as functions of the chemical potential (μ) for periodically segmented nanowires with (a) $t_A=0.9\,t$, (b) $t_A=0.8\,t$, (c) $t_A=0.7t$ and (d) $t_A=0.6\,t$, in comparison to those of a periodic nanowire without impurities (gray lines).

blocks follow the Fibonacci sequence with the same parameter of Fig. 16 and (a) $t_A=0.9\,t$, (b) $t_A=0.8\,t$, (c) $t_A=0.7t$ and (d) $t_A=0.6\,t$. Note that the destruction of the quantization in this case is remarkable due to the presence of the Fibonacci ordering. Moreover, the spectra do not have well defined gap structure as in the 1D systems, finding only pseudogaps. The conductance of quasiperiodically segmented nanowires is higher than the corresponding one of the non-segmented Fibonacci nanowire (gray lines in Fig. 15).

5. Conclusions

In this paper, we analyze in detail the effects of site and bond impurities on the electrical conductivity of periodic and bond-Fibonacci systems with macroscopic length, by using the real-space renormalization method for the Kubo–Greenwood formula.

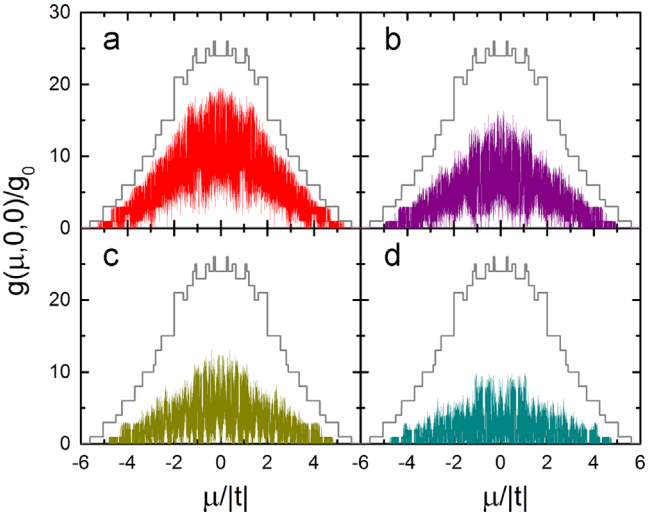

Fig. 17. Conductance (g) spectra as functions of the chemical potential (μ) for quasiperiodically segmented nanowires with (a) $t_A = 0.9\,t$, (b) $t_A = 0.8\,t$, (c) $t_A = 0.7t$ and (d) $t_A = 0.6\,t$, in comparison to that of a periodic nanowire without impurities (gray lines).

For three-dimensional systems the convolution theorem is also employed. It is worth to mention that the method by combining renormalization and convolution does not add extra approximations and it is extremely efficient, whose computing time grows logarithmically with the system length.

For a single impurity in periodic chains, we found that the conductivity spectra are symmetric around the zero chemical potential inside the band, even for a site impurity, which can be seen in the analytic solution of the transmittance for energies within the band given by Eq. (9). In fact, there is an exponentially localized state outside the band, whose conductivity is small enough to be seen in a linear-scale conductivity spectrum. In contrast, for Fibonacci chains, the conductivity spectra are only symmetric with respect to the zero chemical potential when the impurities are of bond nature, while any site impurity produces a notable asymmetry.

In the case of two impurities in periodic chains, we found that the conductivity spectra oscillates and the number of maximums is equal to the number of atoms between the impurities. In fact, the analytical solution of the transmittance obtained in this article for periodic chains with two site impurities confirm this relationship. For Fibonacci chains, the conductivity reduction caused by two impurities is more remarkable when the distance between them is shorter.

The transparent state at the zero chemical potential in Fibonacci chains is always destroyed when site impurities are present. In contrast, for bond impurities, there are transparent states at the zero chemical potential for every three generations when $t_{imp} = t_B$ and the number of impurities is even.

The spectral average of the conductivity depends strongly on the location of the site and bond impurities in periodic chains. Particularly, when the distance between impurities follows the Fibonacci sequence we found that the spectral average falls following a power law as the number of atoms in the system grows. This fact can be understand if one renormalizes all the atoms between impurities obtaining two effective hopping parameters $\tilde{t}(\mu, d_A)$ and $\tilde{t}(\mu, d_B)$. These new hopping parameters are ordered following the Fibonacci sequence and then one obtains a power-law decay behavior with the system length. For segmented periodic chains, the spectral average of the conductivity has a constant behavior with respect to the number of atoms in the system, and has a lower value than that of a periodic chain without block structure.

In the case of periodic nanowires, the conductance quantized spectrum is less destroyed for a single site-impurity plane than for a single bond-impurity one. This destruction is enhanced when two impurity planes are introduced. At the same time, we found resonant conductance peaks for the case of two bond-impurity planes, whose conductance is higher than that of a single impurity plane. For quasiperiodic nanowires, their conductance spectra are less sensitive to site-impurity planes than bond-impurity ones. Finally, the quantization behavior of the conductance in segmented periodic nanowires remains at extremes of the band and it is easily destroyed at the center of the band. In fact, such quantization disappears in quasiperiodically segmented nanowires.

In summary, the renormalization plus convolution method allows a detailed analysis of the impurity effects on the electronic transport in macroscopic periodic and quasiperiodic chains as well as in nanowires, beyond perturbative studies. This analysis reveals that the position of the impurities could be essential and possesses global effects on the electrical conductivity of whole band, such as the power-law decay of the conductivity when the impurities were placed at sites with separations following the Fibonacci sequence. This fact only can be seen clearly in this analysis carried out in systems with macroscopic length. This study can be extended to multiband models, as developed in Ref. [24] for Fibonacci superlattices, and it was found that the single orbital results could be observed only in the vicinity of the superlattice Γ point.

Acknowledgments

This work has been partially supported by UNAM IN113813 and IN113714 and CONACyT 131596. One of the authors (C.R.) thanks the Program of Post-Doctoral Scholarships in the UNAM. Computations were performed at Miztli of DGTIC-UNAM and the technical assistance by Silvia Franco is fully acknowledged.

References

[1] C. Joachim, J.K. Gimzewski, A. Aviram, Nature 408 (2000) 541.
[2] J.C. Ellenbogen, J.C. Love, Proc. IEEE 88 (2000) 386.
[3] Y. Cui, Q. Wei, H. Park, C.M. Lieber, Science 293 (2001) 1289.
[4] F. Patolsky, G. Zheng, O. Hayden, M. Lakadamyali, X. Zhuang, C.M. Lieber, Proc. Natl. Acad. Sci. USA 101 (2004) 14017.
[5] P. Gambardella, M. Blanc, H. Brune, K. Kuhnke, K. Kern, Phys. Rev. B 61 (2000) 2254.
[6] J.V. Barth, G. Costantini, K. Kern, Nature 437 (2005) 671.
[7] M. Ryu, T. Kizuka, Jpn. J. Appl. Phys. 45 (2006) 8952.
[8] R.H.M. Smit, C. Untiedt, A.I. Yanson, J.M. van Ruitenbeek, Phys. Rev. Lett. 87 (2001) 266102.
[9] H. Ohnishi, Y. Kondo, K. Takayanagi, Nature 395 (1998) 780.
[10] A.I. Yanson, G. Rubio-Bollinger, H.E. van den Brom, N. Agraït, J.M. van Ruitenbeek, Nature 395 (1998) 783.
[11] G. Rubio-Bollinger, S.R. Bahn, N. Agraït, K.W. Jacobsen, S. Vieira, Phys. Rev. Lett. 87 (2001) 026101.
[12] E. Scheer, N. Agraït, J.C. Cuevas, A.L. Yeyati, B. Ludoph, A. Martín-Rodero, G.R. Bollinger, J.M. van Ruitenbeek, C. Urbina, Nature 394 (1998) 154.
[13] K. Hansen, S.K. Nielsen, M. Brandbyge, E. Lægsgaard, I. Stensgaard, F. Besenbacher, Appl. Phys. Lett. 77 (2000) 708.
[14] J. van Ruitenbeek, E. Scheer, H. Weber, in: G. Cuniberti, G. Fagas, K. Richter (Eds.), Introducing Molecular Electronics, Springer, Berlin, 2005, pp. 253–274.
[15] V. Rodrigues, T. Fuhrer, D. Ugarte, Phys. Rev. Lett. 85 (2000) 4124.
[16] E. Maciá, ISRN Condens. Matter Phys. 2014 (2014) 165943.
[17] B. Kramer, A. MacKinnon, Rep. Prog. Phys. 56 (1993) 1469.
[18] R. Oviedo-Roa, L.A. Perez, C. Wang, Phys. Rev. B 62 (2000) 13805.
[19] V. Sánchez, C. Wang, Phys. Rev. B 70 (2004) 144207.
[20] Y. Imry, R. Landauer, Rev. Mod. Phys. 71 (1999) S306.
[21] T. Wunderlich, B. Akgenc, U. Eckern, C. Schuster, U. Schwingenschlo, Sci. Rep. 3 (2013) 2605.
[22] D. Nozaki, H.M. Pastawski, G. Cuniberti, New J. Phys. 12 (2010) 063004.
[23] Y. Peng, T. Cullis, I Luxmoore, B. Inkson, Nanotechnology 22 (2011) 245709.
[24] K. Hirose, D.Y.K. Ko, H. Kamimura, J. Phys.: Condens. Matter 4 (1992) 5947.
[25] V. Sanchez, L.A. Perez, R. Oviedo-Roa, C. Wang, Phys. Rev. B 64 (2001) 174205.
[26] J.M. Luck, C. Godreche, A. Janner, T. Janssen, J. Phys. A: Math. Gen. 26 (1993) 1951.
[27] C. Wang, F. Salazar, V. Sanchez, Nano Lett. 8 (2008) 4205.